



Ionizable lipid nanoparticles for RAS protease delivery to inhibit cancer cell proliferation

Ella Atsavapranees^{a,1}, Rebecca M. Haley^{a,1}, Margaret M. Billingsley^a, Alexander Chan^a, Biao Ruan^b, Christian G. Figueroa-Espada^a, Ningqiang Gong^a, Alvin J. Mukalel^a, Philip N. Bryan^{b,c}, Michael J. Mitchell^{a,d,*}

^a Department of Bioengineering, University of Pennsylvania, Philadelphia, PA 19104, USA

^b Potomac Affinity Proteins, LLC, North Potomac, MD 20878, USA

^c Institute for Bioscience and Biotechnology Research, University of Maryland, Rockville, MD 20850, USA

^d Penn Institute for RNA Innovation, Perelman School of Medicine, University of Pennsylvania, Philadelphia, PA 19104, USA

ARTICLE INFO

Keywords:

Lipid nanoparticles
cancer
RAS
Protein therapeutics
Drug delivery

ABSTRACT

Mutations in RAS, a family of proteins found in all human cells, drive a third of cancers, including many pancreatic, colorectal, and lung cancers. However, there is a lack of clinical therapies that can effectively prevent RAS from causing tumor growth. Recently, a protease was engineered that specifically degrades active RAS, offering a promising new tool for treating these cancers. However, like many other intracellularly acting protein-based therapies, this protease requires a delivery vector to reach its site of action within the cell. In this study, we explored the incorporation of cationic lipids into ionizable lipid nanoparticles (LNPs) to develop a RAS protease delivery platform capable of inhibiting cancer cell proliferation *in vitro* and *in vivo*. A library of 13 LNPs encapsulating RAS protease was designed, and each formulation was evaluated for *in vitro* delivery efficiency and toxicity. A subset of four top-performing LNP formulations was identified and further evaluated for their impact on cancer cell proliferation in human colorectal cancer cells with mutated KRAS *in vitro* and *in vivo*, as well as their *in vivo* biodistribution and toxicity. *In vivo*, both the concentration of cationic lipid and type of cargo influenced LNP and cargo distribution. All lead candidate LNPs showed RAS protease functionality *in vitro*, and the top-performing formulation achieved effective intracellular RAS protease delivery *in vivo*, decreasing cancer cell proliferation in an *in vivo* xenograft model and significantly reducing tumor growth and size. Overall, this work demonstrates the use of LNPs as an effective delivery platform for RAS proteases, which could potentially be utilized for cancer therapies.

1. Introduction

The RAS oncogene drives a third of all human cancers, causing an estimated one million deaths per year [1]. There are three RAS isoforms (H, K, and N) in humans. KRAS is the most frequently mutated, found primarily in pancreatic, colorectal, and lung cancers [1]. Scientists have long known that activated RAS drives cancer by promoting cell proliferation and evasion of apoptotic signals [2,3]. However, RAS has been called “undruggable,” as it has been challenging to develop effective therapeutics. Oncogenic mutations (e.g., G12D, G12V, G12C, G13D, and Q61R) decrease its GTPase activity, maintaining RAS in the active (GTP-bound) state. This active RAS has no available sites for small molecule

drugs to bind, which is the conventional approach to target intracellular proteins [4].

Despite these difficulties, there has been recent success in developing therapeutics that target specific RAS mutants. Amgen’s Lumakras (sotorasib), which targets the KRAS^{G12C} mutation, has been approved by the U.S. FDA for the treatment of metastatic non-small cell lung cancer [5]. While this is an exciting advance, Lumakras is currently limited in its application, as this specific mutation only accounts for about 13% of non-small cell lung cancer cases. There remains a pressing need to develop alternative approaches that target other oncogenic RAS mutations.

Protein biologics display high specificity and thus have immense

* Corresponding author at: Department of Bioengineering, University of Pennsylvania, 210 South 33rd Street, 240 Skirkanich Hall, Philadelphia, PA 19104, USA.
E-mail address: mjmitch@seas.upenn.edu (M.J. Mitchell).

¹ Contributed equally to this work.

<https://doi.org/10.1016/j.jconrel.2024.05.015>

Received 11 December 2023; Received in revised form 3 May 2024; Accepted 7 May 2024

Available online 14 May 2024

0168-3659/© 2024 Elsevier B.V. All rights reserved, including those for text and data mining, AI training, and similar technologies.

potential to reach difficult targets like RAS [6]. To introduce new and effective therapies targeting RAS-driven tumor growth, a novel protease (referred to as RAS protease) was recently engineered to cleave active RAS [7]. The protease targets all three isoforms of RAS by recognizing the amino acid sequence QEEYSAM—exposed only when RAS binds GTP [5]. This enables the protease to specifically target active RAS, reducing potential adverse side effects.

To further increase specificity, the RAS protease was designed to enable inducible control of its proteolytic activity. Two inducible versions of the RAS protease were developed: one activated by imidazole, which is benign and not normally present in cells, and another activated by nitrite, which is typically elevated in RAS-driven cancers [8–10] and reaches concentrations of >100 μM in tumor cells [11,12]. Most small molecule drugs inhibit their target by binding or covalent action, making them effective only when stoichiometric amounts of the drug are present intracellularly. In contrast, the RAS protease can act effectively even if the amount of substrate greatly exceeds that of the protease.

While this therapy has immense potential, the RAS protease is currently limited by delivery challenges. Unlike small molecule drugs, which can readily cross the cell membrane, free proteins require delivery systems for uptake into cells, as well as protection from degradation or quick clearance from the circulatory system. Ionizable lipid nanoparticles (LNPs) have recently emerged as a promising platform to achieve potent cytosolic delivery of therapeutic cargo. The success of LNP platforms has led to the U.S. FDA approval of Alnylam's siRNA therapeutic Onpattro and wide usage of the Moderna and Pfizer-BioNTech COVID-19 mRNA vaccines [13–15]. LNPs are traditionally used to deliver nucleic acids, such as messenger RNA (mRNA), small interfering RNA (siRNA), and microRNA (miRNA) [16–18]. Several of these studies have developed LNPs encapsulating siRNA to control tumor growth by regulating the expression of RAS via RNA interference [19,20]. To improve delivery of nucleic acids to the target site and decrease tumor growth *in vivo*, LNPs have been modified with tumor-homing and penetrating lipids [21–24]. miRNA has also been explored to target RAS-driven cancer cell proliferation [25,26]. For these approaches, co-targeting signaling pathways and transcription factors, such as TGF- β ²⁰ and GATA2 [27], has the potential to improve therapeutic outcomes and overcome drug resistance [28]. Recent work has also expanded the application of LNPs to include non-traditional cargos such as proteins [29–33]. Engineered Designed Ankyrin Repeat Proteins (DARPs) targeting RAS were encapsulated and delivered with LNPs, reducing tumor growth *in vivo* [32,33].

Here, we developed an LNP platform to improve the intracellular delivery of a RAS protease to reduce cancer cell proliferation. In doing so, this study examined the role that cationic lipids play in the delivery of protein cargo, as well as their impact on LNP fate *in vivo*. A library of LNPs was designed—based on a previously optimized and published formulation [33]—and each formulation was evaluated for *in vitro* delivery efficiency and toxicity. A subset of LNP formulations was further explored for their impact on cancer cell proliferation in human colorectal cancer cells with the KRAS^{G13D} mutation *in vitro* and *in vivo*, as well as their *in vivo* biodistribution and toxicity. Ultimately, LNPs with a higher concentration of cationic lipid achieved more potent intracellular delivery with minimal toxicity *in vitro* and *in vivo*, enabling a decrease in cancer cell proliferation.

2. Materials and methods

2.1. Ionizable lipid synthesis

The ionizable lipid used in this study (C14-4, structure found in Fig. S1) was synthesized by reacting epoxide-terminated alkyl chains (Avanti Polar Lipids; Alabaster, AL) with polyamine cores (Enamine; Monmouth Jct, NJ) using nucleophilic addition/SN2 reactions, as previously described [34–37]. Components were combined with a 7-fold excess of alkyl chains and mixed for 48 h at 80 °C. The crude product

was transferred to a Rotavapor R-300 (BUCHI; Newark, DE) for solvent evaporation, and the lipids were suspended in ethanol for use in formulation.

2.2. Lipid nanoparticle formulation

Ionizable lipid nanoparticles (LNPs) were synthesized through mixing of an ethanol phase and aqueous phase in a microfluidic device with a 1:3 volume ratio using pump33DS syringe pumps (Harvard Apparatus; Holliston, MA) [38]. The ethanol phase contained C14-4 ionizable lipid, 1,2-dioleoyl-sn-glycero-3-phosphoethanolamine (DOPE) (Avanti Polar Lipids; Alabaster, AL), cationic lipid (Avanti Polar Lipids), cholesterol (Avanti Polar Lipids), and 1,2-dimyristoyl-sn-glycero-3-phosphoethanolamine-N-[methoxy(polyethylene glycol)-2000] (PEG) (Avanti Polar Lipids). For protease LNPs, the aqueous phase contained a solution of 1 \times phosphate-buffered saline (PBS) with 150 mM sodium chloride (pH 5) and purified RAS protease. For mRNA LNPs, the aqueous phase contained 10 mM citric acid and luciferase mRNA at 1 mg/mL (TriLink BioTechnologies; San Diego, CA). For uptake studies, the protease was labeled with DyLight 755 NHS Ester amine-reactive dye (Thermo Fisher Scientific; Waltham, MA). After synthesis, LNPs were subsequently dialyzed against 1 \times PBS in 20 kDa molecular weight cutoff dialysis cassettes for 1 h to remove ethanol.

2.3. Library design

The LNP library screen evaluated the incorporation of four cationic lipids: 1,2-dioleoyl-3-trimethylammonium-propane (DOTAP), 1,2-di-O-octadecyl-3-trimethylammonium propane (DOTMA), dimethyldioctadecylammonium (DDAB), and N-(2-hydroxyethyl)-N,N-dimethyl-2,3-bis(oleoyloxy)propan-1-aminium bromide (DORI) (Avanti Polar Lipids; Alabaster, AL). The cationic lipid was substituted into a base formulation [33] at molar percentages of 10%, 20%, and 30% relative to C14-4 ionizable lipid. The lipids were combined with set ratios of cholesterol, phospholipid, and lipid-anchored PEG.

2.4. Dynamic light scattering and surface zeta potential

10 μL of LNPs were diluted 100 \times in 1 \times PBS and measured in 4 mL disposable cuvettes by dynamic light scattering (DLS) on the Zetasizer Nano (Malvern Instruments; Malvern, UK). LNP size (Z-average diameter) and polydispersity index (PDI) are reported as the mean \pm standard deviation ($n = 3$ measurements). To quantify surface zeta potential, 20 μL of LNPs were diluted 50 \times in water and measured in DTA1070 zeta potential cuvettes (Malvern Panalytical, Malvern, UK) on the Zetasizer Nano. To quantify surface zeta potential of the RAS protease, proteins were diluted 500 \times .

2.5. LNP pK_a

pK_a values of the LNPs were measured using 6-(p-toluidino)-2-naphthalenesulfonic acid (TNS) assays. Buffered solutions of 150 mM sodium chloride, 20 mM sodium phosphate, 25 mM ammonium citrate, and 20 mM ammonium acetate were adjusted to reach pH values in increments of 0.5 from 2 to 12. LNPs were added to each pH-adjusted solution in a 96-well plate, and TNS was added to each well for a final TNS concentration of 6 μM . The resulting fluorescence was measured on the Infinite M Plex plate reader. The resulting data was fit with a sigmoidal regression, and pK_a was calculated as the pH at which the fluorescence intensity reached 50% of its maximum value. Data are reported as the mean \pm standard deviation ($n = 3$ measurements).

2.6. Protease expression and purification

The proteases used in this study are highly engineered subtilisins from *Bacillus amyloliquefaciens* denoted RASProtease(I) (PDB codes

6U9L 6UAO 6UAI) and RASProtease(N) [7]. To promote encapsulation into cationic LNPs, an acidic cellulose binding domain (PDB code 5E9P) was fused to the C-terminus of each protease [39]. Expression was carried out in *E. coli* by auto-induction, and purification was performed by affinity chromatography using a cognate 7-mer peptide purchased from AnaSpec, Inc., as previously described [7].

Both proteases were previously engineered to require a cofactor for activity [7]. RASProtease(I) is activated by imidazole, allowing protease activity to be regulated by a xenobiotic compound. RASProtease(N) is activated by nitrite. Elevated nitrite occurs in many disease states including RAS-related cancers [8,12]. The imidazole-activated protease was used for all *in vitro* experiments and *in vivo* biodistribution experiments, and either the imidazole or nitrite-activated protease was used for tumor model experiments.

2.7. LNP protease concentration and activity

Protease concentration within the LNP sample was determined using a micro-BCA protein assay as per the manufacturer instructions (Thermo Fisher Scientific; Waltham, MA). LNPs were diluted in PBS with 2% SDS to accommodate the presence of lipids in the sample. BCA working reagent was added to each sample, and samples were incubated for 2 h at 37 °C in a sonicating bath to allow for quantification of encapsulated as well as free or surface-anchored protein. For studies interested in free and surface-anchored protein only, static conditions were used at the same temperature and time. Samples were added in triplicate to 96-well plates, and the resulting absorbance was measured on a plate reader alongside a standard curve to quantify protein concentration. Concentration values are reported as the mean \pm standard deviation ($n = 3$ measurements). To measure protease activity, 0.1% Triton X-100 was added to LNPs (1:100 dilution in 1 \times PBS) to release the protease cargo. LNPs were incubated with 1 μ M QEEYSGM-AMC and 10 mM imidazole. When active, the protease recognizes the amino acid sequence QEEY-SAM and cleaves AMC from the peptide, allowing it to fluoresce in solution. AMC fluorescence ($\lambda_{\text{ex}}/\lambda_{\text{em}} = 341/441$ nm) was measured over 42 min using a plate reader.

2.8. LNP protease encapsulation via size exclusion chromatography

Encapsulation efficiency was evaluated by separating free and encapsulated DyLight-labeled RAS protease by size exclusion. A size exclusion chromatography column packed with 22 cm of Sepharose CL-4B resin was used to separate LNP from free protein. Resulting fractions were mixed with equal volumes of 0.1% Triton-X in black 96-well plates, and fluorescence was measured in a plate reader. Resulting peaks were integrated in GraphPad Prism to determine the area under the curve. For 30% DOTAP (filtered) samples, fractions containing LNP—determined by absorbance on a NanoQuant plate (Tecan; Switzerland)—were collected and combined for future use.

2.9. Cell culture

Human colorectal cancer cells (HCT116) were cultured in McCoy's 5A media with L-glutamine (Thermo Fisher Scientific; Waltham, MA), supplemented with 10% fetal bovine serum (FBS) and 1% penicillin-streptomycin (P/S), and maintained in a 5% CO₂, 37 °C humidified incubator. The cells were gifted by Michael Farwell.

2.10. Flow cytometry

Cells were seeded in 24-well plates at 70,000 cells in 700 μ L of media. After 48 h, LNPs were added to the cells at the desired concentration. For cell proliferation assays, CellTrace Far Red reagent (Thermo Fisher Scientific; Waltham, MA) was added prior to LNPs as per the manufacturer's instructions. Cells were incubated for 24 h before functional readout assays were performed. Cells were washed once with

cold PBS, detached with 0.25% trypsin, and pelleted in a 4 °C tabletop centrifuge at 300 rcf. Cell pellets were resuspended in PBS, SYTOX green was added according to manufacturers instructions, and samples were analyzed on the BD LSR II Flow Cytometer (BD Biosciences; Franklin Lakes, NJ). At least 10,000 total events were collected. Data was analyzed with FlowJo v10 (BD Biosciences) and reported as the mean \pm standard deviation ($n = 3$ measurements). Data reported is of live cells only, as determined by the gating scheme shown in Fig. S2.

2.11. In vitro toxicity assays

Cells were seeded in 96-well plates at 10,000 cells in 75 μ L of media. After 48 h, LNPs without imidazole (100 nM) were added to the wells. To assess toxicity from imidazole alone, imidazole was added to the cells at concentration increments from 0 to 10 mM. Cells were incubated for 24 h, and 75 μ L of CellTiter-Glo™ (Promega) was added to each well. Following incubation for 10 min, luminescence was measured using a plate reader. Luminescence was normalized within each plate to untreated cells and reported as the mean \pm standard deviation ($n = 3$ measurements).

2.12. Biodistribution analysis

All LNPs were concentrated using Amicon Ultra centrifugal filters (100 kDa MWCO, Millipore Sigma) and labeled with DiR (Thermo Fisher Scientific; Waltham, MA). Black mice (C57BL/6 J) were treated with either luciferase mRNA LNPs (0.5 mg/kg) or DyLight 650-labeled RAS protease LNPs (1 mg/kg) *via* intravenous (IV) injections. mRNA LNPs received a lower weight-based dosage to represent more similar lipid and particle concentrations between the two LNP formulation and cargo types, so that DiR fluorescence would remain within similar ranges. After 6 h, mice were sacrificed, blood was collected, and organs were excised and imaged using the *in vivo* imaging system (IVIS) Spectrum (PerkinElmer; Waltham, MA). Mice receiving luciferase mRNA LNPs also received IP injection of Luciferin (3 mg per mouse) Normalized luminescence and fluorescence values are reported as the mean \pm standard deviation ($n = 3$ measurements).

2.13. In vivo toxicity assays

Blood was collected from black mice (C57BL/6 J) treated with either mRNA LNPs (0.5 mg/kg) or RAS protease LNPs (1 mg/kg) *via* IV injections. A mouse ELISA kit (R&D Systems; Minneapolis, MN) was used to evaluate IL-6 and TNF- α levels 6 h following LNP or PBS treatment in the serum as per the manufacturer's instructions. Concentration values are reported as the mean \pm standard deviation ($n = 3$ measurements).

2.14. Tumor model

HCT116 cells expressing EGFP (3×10^6) [6] were resuspended in PBS and injected subcutaneously into the flanks of nude (Nu/J) mice. Once tumors were >10 mm³ (day 9), LNP injections began. 1 mg/kg or 0.5 mg/kg of RAS protease (either free in PBS or encapsulated using LNPs) was injected intratumorally every day. Tumors were measured using calipers before each injection. At the endpoint (day 15), mice were sacrificed, and tumors were excised and imaged using the IVIS Spectrum (PerkinElmer) to quantify EGFP fluorescence. Excised tumors were measured in three dimensions using calipers and weighed. Data are reported as the mean \pm standard deviation.

3. Results and discussion

3.1. Design and synthesis of RAS protease LNP library

LNPs are typically composed of four main components in addition to their cargo: ionizable lipid, phospholipid, cholesterol, and lipid-

anchored polyethylene glycol (PEG) [40]. The ionizable lipid remains neutral at physiological pH but becomes positively charged in acidic environments to aid in endosomal escape and enable potent intracellular delivery [41,42]. Coating the surface of LNPs with PEG has been shown to improve delivery efficiency and prolong systemic circulation time by shielding LNPs from aggregation, opsonization, and phagocytosis [43]. In some LNP formulations, a fifth component—a cationic lipid—is introduced. This serves to improve protein encapsulation and can influence *in vivo* fate in some cases. In this study, we formulated a library of 13 LNPs using four different commercially available cationic lipids as the fifth component: DOTAP, DOTMA, DDAB, and DORI (Fig. 1). As the basis for this library, we used a previously published formulation (B6 [33]) which was optimized for intracellular delivery of a small protein RAS inhibitor. These LNPs were evaluated for the delivery of an engineered RAS protease to inhibit proliferation of human colorectal cancer (HCT116) cells, which have the KRAS^{G13D} mutation. Previous studies have shown that the incorporation of strong negative charge to protein cargos can aid in LNP encapsulation and stability [32,33,44]. For this work, an acidic cellulose binding domain was fused to the C-terminus of the RAS protease to aid in encapsulation. This allows the protease to more closely resemble traditional nucleic acid cargos, which have a strong negative charge. The modified RAS protease has been characterized and evaluated in previously published work [7] and maintains its catalytic parameters after modification, with no change in activity before and after the addition of the acidic cellulose binding domain.

LNPs were synthesized using microfluidic mixing of an ethanol phase—containing ionizable lipid (C14-4), phospholipid (DOPE), cationic lipid, cholesterol, and lipid-anchored PEG—with an aqueous phase containing the RAS protease. Several studies have demonstrated that ionizable lipid structure greatly impacts LNP delivery, and cationic lipids have been of interest recently due to their impact on *in vivo* distribution [31,34]. However, even though cationic lipids have become more widely used, there is still limited information about their role in protein encapsulation with LNPs, including whether these *in vivo* effects remain consistent with these cargos [34]. This study explored the incorporation of cationic lipids into LNPs to develop a RAS protease delivery platform to inhibit cancer cell proliferation.

3.2. *In vitro* screen of RAS protease LNP library

Based on previous work, we hypothesized that incorporating a higher molar percentage of cationic lipid in LNPs would enable greater interaction with the acidic domain of the RAS protease cargo [33]. A library of 13 LNPs (Table S1) was designed to evaluate the impact of four cationic lipids at molar percentage substitutions of 10, 20, and 30% relative to ionizable lipid. A formulation with no cationic lipid was also included as a control. To enable a fluorescence-based readout of intracellular delivery *via* flow cytometry, the protease was labeled with DyLight amine-reactive dye prior to encapsulation into LNPs. To evaluate *in vitro* delivery efficiency and toxicity, HCT116 cells were treated with either free protease, protease delivered *via* commercially available lipofectamine, or protease LNPs (100 nM) without imidazole.

All LNP formulations with >10% cationic lipid substitution demonstrated a significant improvement in median fluorescence intensity (MFI) relative to the free protease control (Fig. 2A, B). LNP formulations with higher cationic lipid substitution percentages generally resulted in greater intracellular delivery, indicating that the incorporation of cationic lipid is essential for protein encapsulation into LNPs. Each formulation was also evaluated for the percentage of DyLight-positive cells (Fig. 2A). All LNP formulations demonstrated a significant increase in delivery compared to free protease. The top formulations from the *in vitro* screen were 30% DOTAP, 30% DOTMA, and 30% DORI, which demonstrated a 5.5, 4.4, and 5.2-fold increase in MFI relative to free protease and 54.8, 56.7, and 57.8% positive cells, respectively. While the free protease shows minimal intracellular delivery, the LNP significantly improves this into a range where, ideally, a therapeutic effect can be achieved.

To evaluate potential off-target toxicity from LNP dosage, cells were treated with LNPs without an activating cofactor (such as imidazole or nitrite). Only one formulation (10% DORI) significantly decreased cell viability when compared to the 0% cationic lipid control, suggesting that substituting ionizable lipid for cationic lipid into LNPs at molar percentages of <30% generally does not induce cytotoxicity *in vitro* (Fig. 2C). Treating cells with imidazole alone did not induce additional toxicity (Fig. S3). Ultimately, the 30% DOTAP, 30% DOTMA, and 30% DORI formulations significantly increased *in vitro* delivery of the RAS protease to HCT116 cells with no significant changes in LNP toxicity.

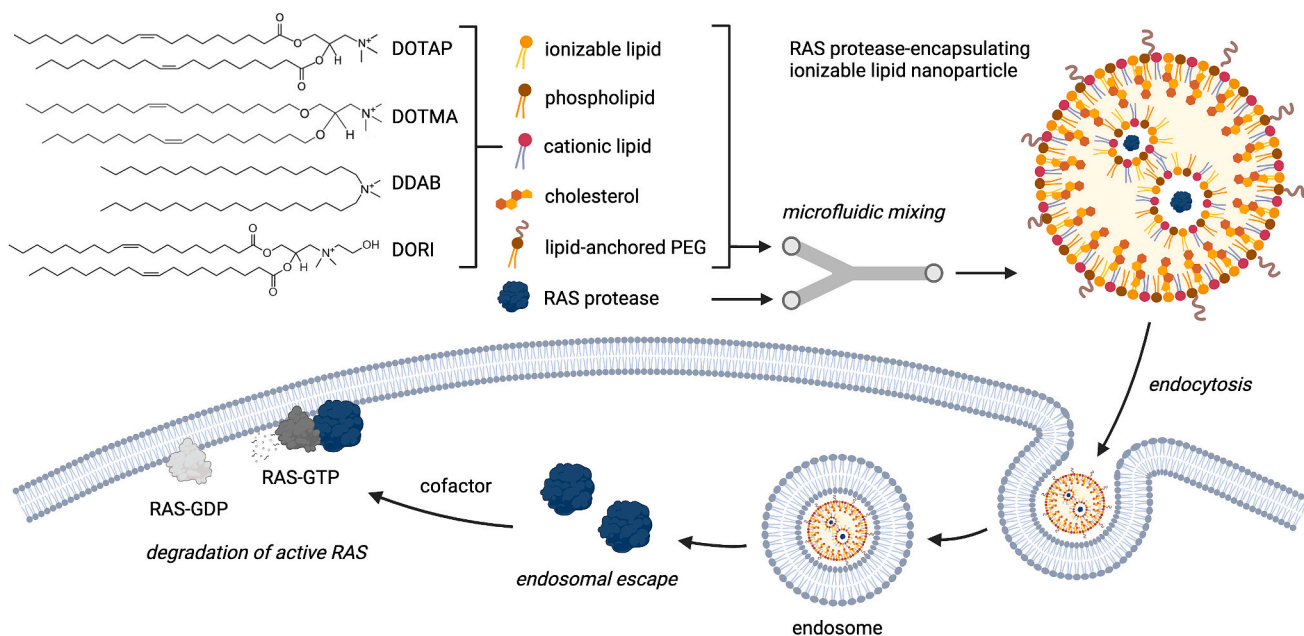
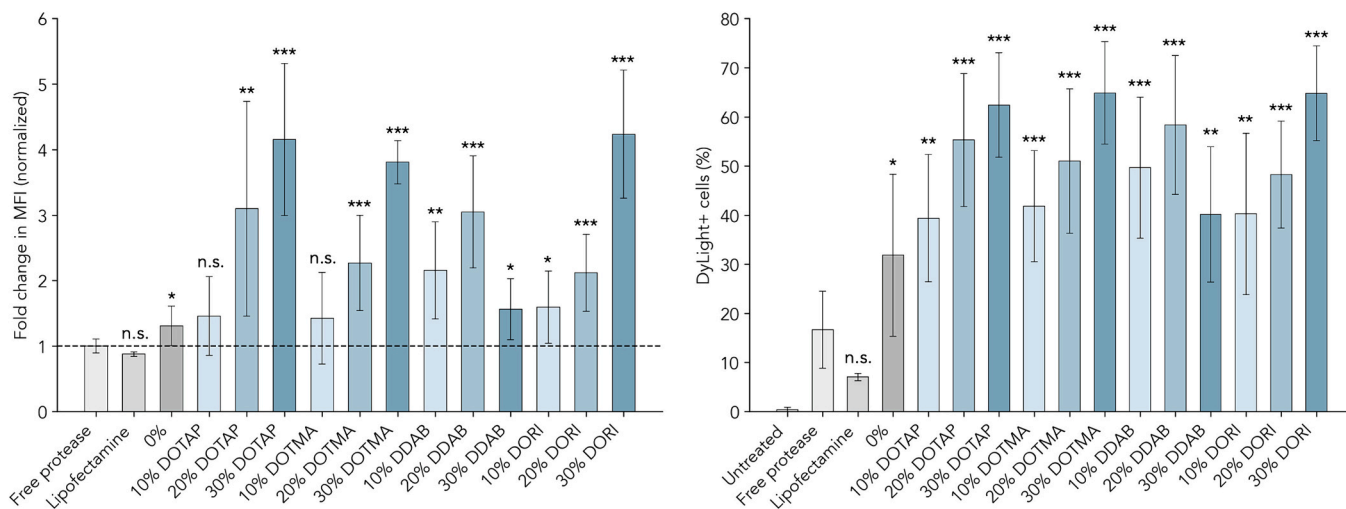
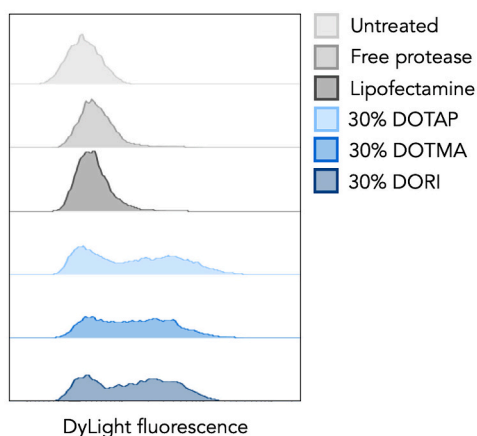


Fig. 1. Schematic of ionizable lipid nanoparticle (LNP) platform to enable delivery of an engineered protease that degrades active RAS to inhibit cancer cell proliferation.

A Intracellular delivery of RAS protease



B



C

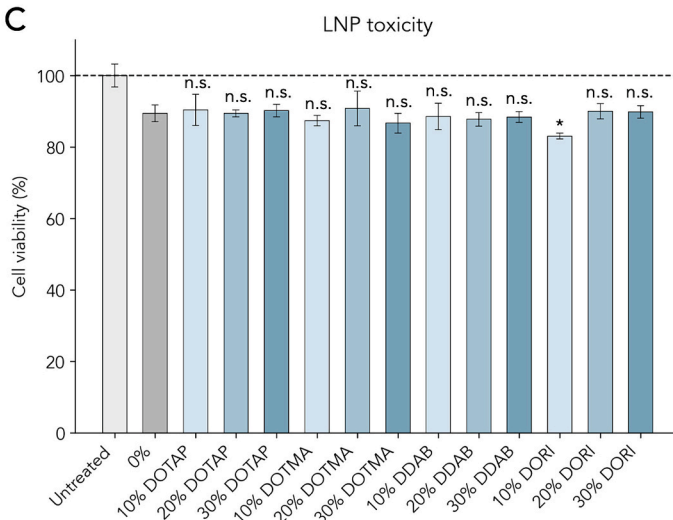


Fig. 2. *In vitro* screen of LNP library for the intracellular delivery of RAS protease to HCT116 cells. (A) Median fluorescence intensity (MFI) per cell relative to free protease for lipofectamine and LNPs. Percentage of DyLight-positive cells for cells without treatment and cells treated with free protease, lipofectamine, and LNPs. (B) Representative flow cytometry histograms. (C) Percent viability of cells treated with LNPs, normalized to untreated cells. RAS protease is inactive without imidazole or nitrite, and any toxicity is thus likely due to LNP components. $n = 3$. Error bars denote standard deviation. An ANOVA was used to determine if treatment group means for MFI and percentage of positive cells differed significantly from the free protease control and if cell viability of LNPs with cationic lipid differed significantly from the 0% formulation containing no cationic lipid (*: $p < 0.05$, **: $p < 0.01$, ***: $p < 0.001$).

3.3. RAS protease LNP characterization

LNPs were characterized by Z-average diameter, polydispersity index (PDI), zeta potential, and pK_a to evaluate if cationic lipid type and substitution percentage influenced physicochemical characteristics (Fig. 3). There were no observable trends in size or PDI based on cationic lipid or substitution percentage. LNPs ranged from 199.2 to 349.2 nm in diameter, and all formulations had a PDI under 0.3 (Fig. 3A, B). LNPs were relatively neutral; interestingly, formulations that did not achieve high delivery efficiencies were generally more negatively charged. This was likely due to free protease in solution from lower LNP encapsulation, as free protease was not removed prior to characterization. Cationic lipid type and substitution percentage did not significantly impact pK_a , which ranged from 6.41 to 6.68 (Fig. 3C).

In addition, LNPs were characterized for protease concentration and encapsulation efficiency. Protease concentration within LNPs was determined using a micro-BCA protein assay. Concentration values ranged from 3.55 to 6.76 μM for all formulations with no observable trends (Table S2). Since the protease is relatively stable under LNP

storage conditions, it is unsurprising that the concentration was consistent across formulations, as there was free protease in these solutions. Therefore, to determine the amount of RAS protease encapsulated into LNPs, size exclusion chromatography (SEC) was used to detect DyLight-labeled protease. Since LNPs are larger than individual proteins, they elute from the column faster, allowing encapsulation efficiency to be determined. The formulation containing 0% cationic lipid did not have an observable LNP peak, indicating that negligible RAS protease was encapsulated. In contrast, both top-performing formulations tested (30% DOTAP and 30% DORI) had distinct protease LNP peaks, with 7.3 and 7.7% encapsulation efficiencies, respectively (Fig. 3D). This encapsulation is significantly less efficient than that of the small protein this LNP system was originally designed for, as the heterogeneity of protein shape, size, and charge necessitates re-optimization for ideal encapsulation efficiency [33]. Specifically, the RAS protease used here is approximately 150% larger, has two distinct regions—due to the cellulose binding domain—and is overall more charged, with localized areas of strong positive and negative charge (Fig. S4).

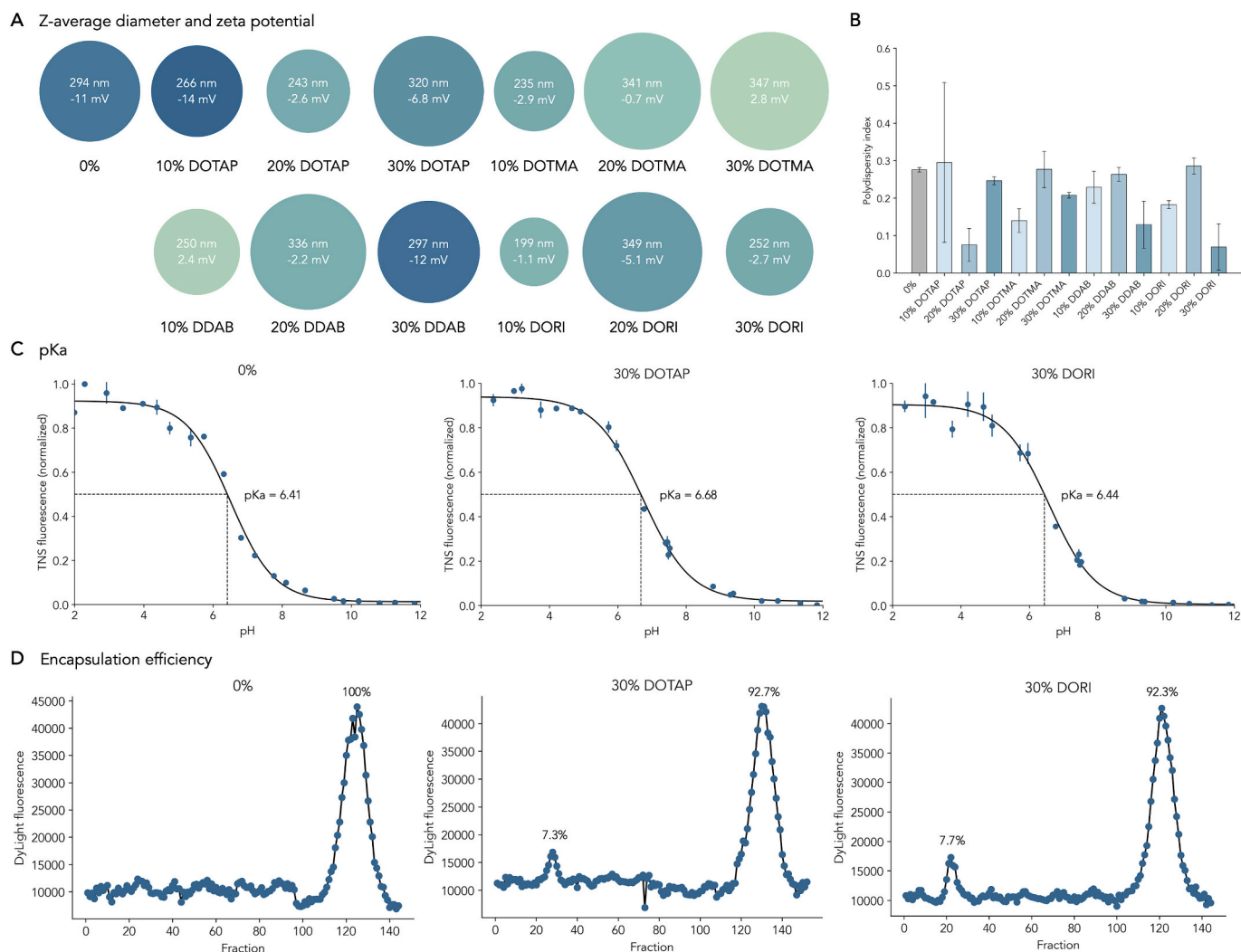


Fig. 3. Characterization of LNP formulations encapsulating RAS protease. (A) Z-average diameter (nm), zeta potential (mV), and (B) polydispersity index (PDI) for all formulations. (C) pKa curves and (D) encapsulation efficiency for 0% and top LNP formulations. $n = 3$ for diameter, PDI, and pKa measurements. Error bars denote standard deviation.

3.4. RAS protease LNP delivery decreases cancer cell proliferation *in vitro*

All LNP formulations containing 30% cationic lipid were evaluated at doses of 1, 10, and 100 nM protease to evaluate any potential differences in dose-responsiveness. This dosing is based on the total value of protein in solution (both encapsulated into LNPs and free protease). There was a significant increase in MFI between doses of 10 and 100 nM in all formulations tested (Fig. 4A, B). Similarly, the percentage of positive cells following treatment with LNPs dramatically increased between doses of 10 and 100 nM (Fig. 4A). This response was similar among all cationic lipid types.

LNP formulations with 30% cationic lipid were further explored for their impact on cancer cell proliferation in HCT116 cells. Cells were treated with LNPs and imidazole, a cofactor to activate the protease. To evaluate RAS activity, CellTrace reagent was added prior to LNP treatment to label cells and monitor multiple generations of proliferating cells using dye dilution (Fig. 4C). This reagent readily diffuses into cells and is cleaved by intracellular esterases to yield a fluorescent compound, which covalently binds to intracellular amines. Since MFI decreases as cells divide, cells with normal proliferation yield a lower MFI, while cells with reduced proliferation yield a higher MFI. Based on this metric, all LNP formulations with 30% cationic lipid resulted in a significant decrease in cancer cell proliferation, as indicated by a higher MFI

compared to the untreated cells (Fig. 4D). Of these formulations, 30% DORI produced the greatest decrease in cancer cell proliferation *in vitro*. To measure RAS degradation, western blotting was used to visualize RAS concentration (Fig. 4E). The 30% DOTAP LNP formulation produced slight reductions in RAS compared to the control bands in both typical and SEC-filtered formats. In the filtered form, all free protease was removed, and lower total protease dosages were used, as the effective encapsulated protease dosage was higher.

To measure proteolytic activity, a nonionic surfactant (Triton X-100) was added to LNPs to release their cargo, and a peptide encoding the protease target (QEEYSAM) and a fluorophore (AMC) was added to the solution with imidazole (Fig. 4F). When the protease cleaves the QEEYSAM-AMC peptide—as it would in targeting RAS-GTP—fluorescence is emitted. All 30% cationic lipid formulations demonstrated an increase in fluorescence over time, indicating that the protease maintained its activity following encapsulation into LNPs. Of the formulations, 30% DOTAP demonstrated the highest level of activity, as indicated by fluorescence over time.

3.5. Cationic lipid and cargo effects for LNP trafficking *in vivo*

Based on *in vitro* results, the incorporation of cationic lipid into LNPs is necessary for effective encapsulation and delivery of the RAS protease.

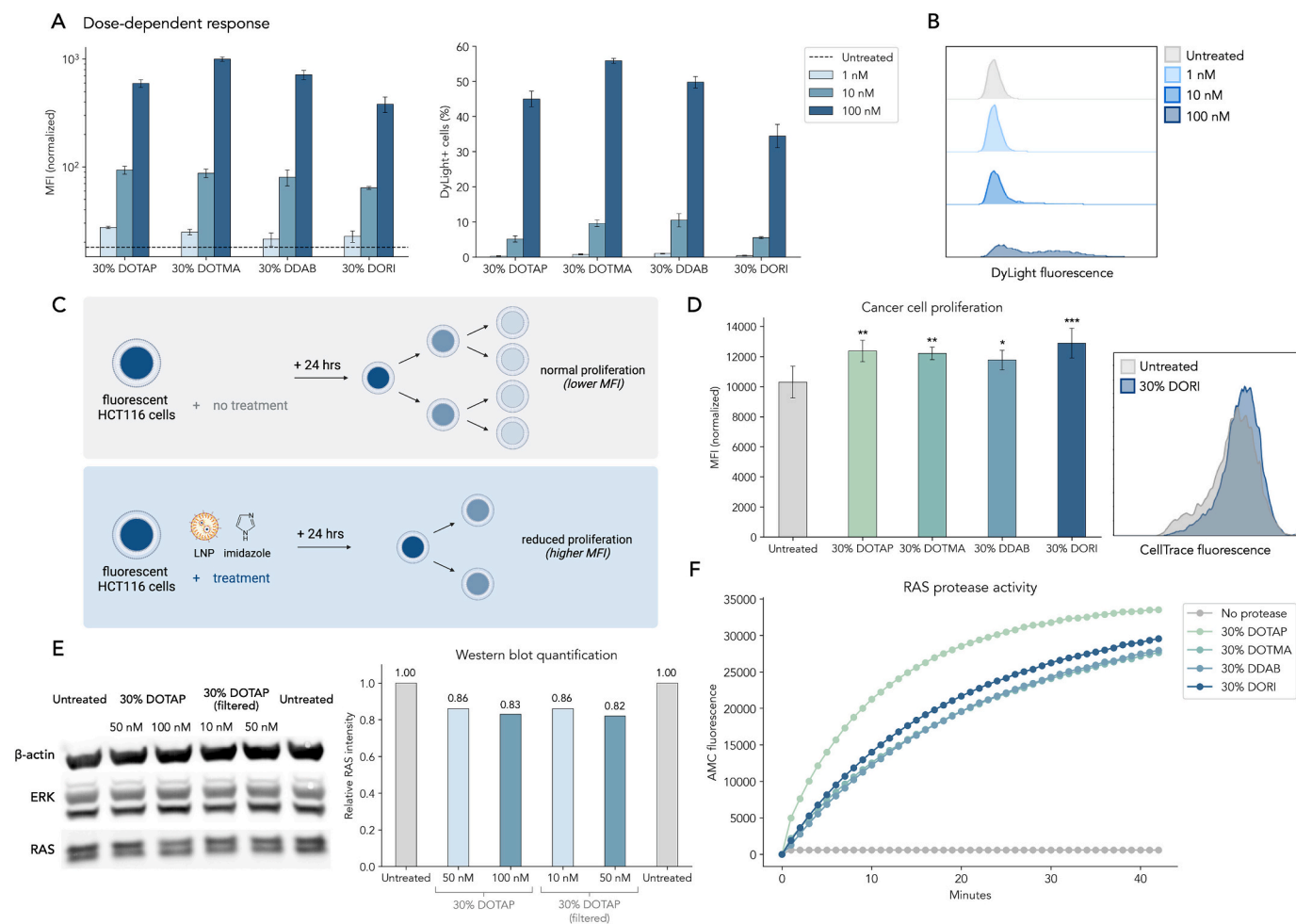


Fig. 4. Dose-dependency and effects on cancer cell proliferation using LNPs with 30% cationic lipid. (A) Median fluorescence intensity (MFI) per cell and percentage of DyLight-positive cells for LNPs at doses of 1, 10, and 100 nM protease. (B) Representative flow cytometry histograms. (C) Schematic of CellTrace cell proliferation assay. (D) MFI for LNPs compared to untreated group and representative flow cytometry histogram. $n = 3$. Error bars denote standard deviation. An ANOVA was used to determine if treatment group means for MFI differed significantly from the untreated group (*: $p < 0.05$, **: $p < 0.01$, ***: $p < 0.001$). (E) Western blot and quantification of cells treated with 30% DOTAP LNPs before and after SEC-filtration at doses of 50 nM and 100 nM or 10 nM and 50 nM protease. (F) Activity of RAS protease encapsulated into LNPs. AMC fluorescence produced by 30% DOTAP, 30% DOTMA, 30% DDAB, and 30% DORI LNP formulations (1:100 dilution) compared to no protease over 42 min.

Recent studies have indicated that cationic lipids significantly impact LNP fate *in vivo*, enabling extrahepatic delivery after systemic administration, but these studies have primarily focused on the delivery of nucleic acids [31,45]. Optimizing protein delivery using LNPs is an active area of research; however, it has not yet reached the same level of clinical success as mRNA and siRNA. In previous work, LNPs with cationic lipids encapsulating small protein cargos retained their traditional liver-tropic biodistribution profile [33]. Therefore, we decided to explore how RAS protease LNPs compared to more traditional mRNA LNPs *in vivo* and whether the incorporation of various cationic lipids resulted in differing fates. We aimed to identify any differences among cationic lipid identities in mRNA LNPs only and test whether previous findings based on cationic lipids—specifically biodistribution to the lungs—would be generalizable or specific to the cargo type.

To evaluate the impact of cationic lipid and cargo on biodistribution, black mice (C57BL/6 J) were treated with either luciferase mRNA LNPs (0.5 mg/kg) or RAS protease LNPs (1 mg/kg) *via* intravenous (IV) injections. For the RAS protease LNPs, this dosing is based on the total value of protease within the sample (both encapsulated into LNPs and free protease). The protease was labeled with DyLight amine-reactive dye and LNPs were labeled with DiR to track both cargo and LNP distribution (Fig. 5A).

In the mRNA LNP groups, normalized luminescence from luciferase mRNA translation was observed in the lungs, liver, and spleen (Fig. 5B). Compared to the 0% cationic lipid formulation, LNP formulations with 30% cationic lipid had increased delivery to the lungs relative to the liver and spleen. This indicates that incorporating cationic lipid into mRNA LNPs increases LNP trafficking to the lungs, an effect that has been previously described [31]. However, the type of extra-hepatic delivery observed varied with alternate cationic lipids. The 30% DOTAP group had relatively less mRNA delivery to the spleen than the other cationic lipids tested as well as the 0% cationic lipid control (Fig. 5B, S5). However, the ratio of luminescence between the liver and lungs was consistent across all cationic lipids.

In the protease LNP groups, normalized DyLight fluorescence from RAS protease distribution was observed in the lungs, liver, spleen, and kidneys (Fig. 5C). RAS protease LNPs demonstrated an even greater increase in lung delivery compared to mRNA LNPs. Again, this supports existing literature demonstrating increased lung delivery with the introduction of cationic lipid. LNP formulations with cationic lipid had increased delivery to the both the lungs and liver compared to the 0% formulation, indicating that the introduction of cationic lipid increases RAS protease delivery overall.

Normalized DiR fluorescence from LNP lipid distribution was

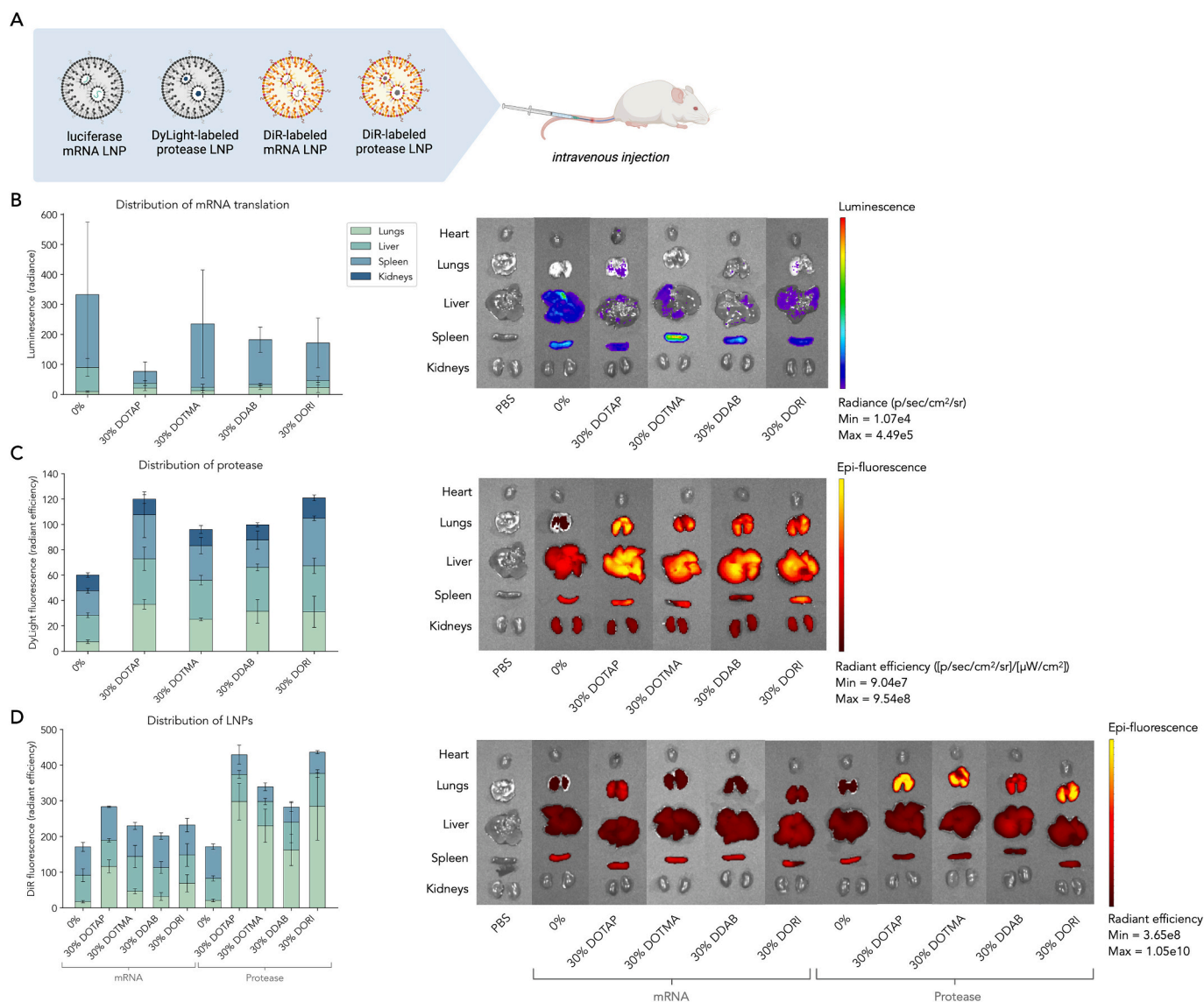


Fig. 5. Biodistribution of luciferase mRNA and RAS protease LNPs in mice (C57BL/6 J). (A) Schematic of biodistribution experiment. (B) Normalized organ luminescence ($\text{p/sec/cm}^2/\text{sr}$) from mRNA expression and IVIS images 6 h after IV injection of mRNA LNPs (0.5 mg/kg). (C) Normalized organ DyLight fluorescence (radiant efficiency) from protease and IVIS images 6 h after IV injection of protease LNPs (1 mg/kg). (D) Normalized organ DiR fluorescence (radiant efficiency) from lipids and IVIS images 6 h after IV injection of mRNA and protease LNPs. $n = 3$. Error bars denote standard deviation.

observed in the lungs, liver, and spleen (Fig. 5D). For both mRNA and RAS protease LNPs, formulations with cationic lipid increased lipid accumulation in the lungs. Incorporating cationic lipid into LNPs did not significantly affect DiR fluorescence in the liver for either mRNA and RAS protease LNPs nor fluorescence in the spleen for mRNA LNPs. Interestingly, RAS protease LNPs without cationic lipid had greater accumulation of lipids in the spleen than formulations with cationic lipid. The presence of DyLight (protease) but not DiR (LNP) in the kidneys indicates that there was no LNP delivery to the kidneys. Rather, free protease in the LNP solution or cleaved DyLight dye was filtered from the bloodstream post-injection. Both 0% cationic lipid formulations (protease and mRNA) had similar organ ratios (liver-to-lungs, spleen-to-lungs, and spleen-to-liver). The introduction of cationic lipid decreased liver-to-lung and spleen-to-lung LNP distribution for both cargo types, although this decrease was more significant for protease LNPs.

When delivered intravenously to xenograft tumor-bearing mice, RAS protease LNPs did not result in significant RAS protease accumulation at the tumor site (Fig. S6A). In fact, fluorescence at the tumor site was highest in the free protease (no LNP) group, indicating that free protease

or cleaved DyLight dye was more capable of crossing into the tumor microenvironment from the bloodstream than LNPs, which are much larger.

Overall, the distribution of LNPs *in vivo* was similar for the two cargos when no cationic lipid was incorporated. However, the introduction of cationic lipid induced changes in distribution that were primarily dependent on the cargo (Fig. 5D), indicating that published cationic lipid trends may not be generalizable to all cargo types. Introducing cationic lipid into LNPs increased delivery to the lungs, especially for the RAS protease. While protease LNPs with cationic lipid improved delivery overall, mRNA LNPs with cationic lipid did not improve mRNA expression but did promote extra-hepatic delivery.

3.6. Cationic lipid type minimally impacts LNP toxicity

The introduction of permanent positive charge in the form of cationic lipids has been previously shown to improve delivery of protein cargos and alter biodistribution of LNPs [31,33,46]. However, there have also been recent reports of increased toxicity when cationic lipids are used in

in vivo. Specifically, clotting in the lungs has been identified as a serious side effect at high dosages [45]. Therefore, it is important to identify potential changes in this toxicity with alternate cationic lipids, as DOTAP has been the primary lipid used in these preliminary studies.

To identify potential large-scale differences in immune response among the cationic lipids as well as differences caused by cargo type, the concentrations of inflammatory cytokine markers 6 h after LNP administration were evaluated. IL-6 and TNF- α concentrations in mouse serum after treatment with either mRNA or RAS protease LNPs were measured *via* an ELISA to evaluate potential *in vivo* toxicity (Fig. 6A, B). Elevated levels of IL-6 and TNF- α can indicate signs of cytotoxicity and inflammation, particularly in the liver. None of the LNP formulations produced significant increases in IL-6 levels compared to the PBS control. However, the 0%, 30% DDAB, and 30% DORI mRNA formulations showed significant increases in TNF- α . When repeated in mice bearing xenograft tumors, all RAS protease LNPs showed similar or reduced IL-6 and TNF- α serum levels compared to the PBS control (Fig. S7). This suggests that substituting ionizable lipid for cationic lipid into RAS protease LNPs at molar percentages of <30% does not induce significant cytotoxicity at these dosages, based on this metric.

3.7. Top LNP formulation decreases cancer cell proliferation *in vivo*

To evaluate the impact of RAS protease LNP delivery on cancer cell proliferation *in vivo*, HCT116 cells expressing EGFP were injected subcutaneously into the flanks of nude (Nu/J) mice (Fig. 7A). After tumors reached 10 mm³, mice were injected intratumorally every day for a week with either PBS or RAS protease (1 mg/kg, free in PBS or within LNP sample). For the RAS protease LNPs, this dosing is based on the total value of protease within the sample (both encapsulated into LNPs and free protease). For the groups treated with the nitrite-activated protease, no cofactor was added, as nitrite is naturally found in the tumor microenvironment. For groups treated with the imidazole-activated protease, imidazole was also injected.

Based on time-course distribution of the RAS protease—delivered *via* the 30% DOTAP formulation—the majority of RAS protease remained in the tumor microenvironment after intratumoral (IT) injection (Fig. S6C). This resulted in a high local concentration of RAS protease LNP with minimal off-target effects. At the endpoint of the experiment, normalized EGFP and tumor volume were measured. Both 30% DOTAP

formulations—encapsulating nitrite-activated or imidazole-activated RAS protease—demonstrated a significant decrease in normalized EGFP fluorescence of HCT116 cells compared to the untreated (PBS) group (Fig. 7B).

None of the LNP formulations demonstrated a significant decrease in tumor volume compared to the untreated group, although both 30% DOTAP formulation groups appeared to have slightly decreased sizes (Fig. S8). It is possible that, since the LNPs were injected intratumorally, the RAS protease only affected the interior of the solid tumor. Without cell debris clearance at the tumor site, differences in tumor volume may be minimal, even when tumor progression is successfully inhibited in the tumor interior. Thus, EGFP expression of tumor cells may be a more sensitive measurement of RAS protease activity.

Due to the low encapsulation efficiency of these LNP formulations, we hypothesized that a significant contributor to the limited decrease in tumor size was that the dosage of encapsulated protease was significantly lower than the total protease dosage. To test this, the tumor model was repeated with the top-performing formulation—30% DOTAP—filtered using SEC to remove free protease. Fractions containing LNP were collected and fractions containing excess free protease were discarded. To confirm that all free protease was successfully removed, a micro-BCA assay was used to quantify the approximate protein concentration in a static and sonicated state. In the static state, only free proteins or proteins conjugated to the surface react with the working reagent. In the sonicated state, all proteins, regardless of encapsulation, react. From this assay, we found that the initial 30% DOTAP formulation contained $9.9 \pm 0.4 \mu\text{M}$ (expected $10.9 \mu\text{M}$ assuming perfect mixing and no loss) and 68% of that protein was available to react with the micro-BCA reagent under static conditions. In contrast, the filtered LNPs contained $0.64 \pm 0.01 \mu\text{M}$ (expected $0.79 \mu\text{M}$ assuming perfect mixing and no loss, based on calculated encapsulation efficiency of 7.3%) and only 39% of that protein was available to react with the micro-BCA reagent under static conditions (Fig. S9).

For the *in vivo* tumor model, all conditions remained the same as the original experiment, with the exception that the filtered 30% DOTAP LNP was dosed at a total protease concentration of 0.5 mg/kg, as the number of LNPs in solution limited concentration. Under these conditions, we saw inhibition in tumor progression (Fig. 7D) and a significant decrease in tumor volume (Fig. 7E). Due to one nonresponsive tumor, reductions in cancer cell activity (measured by EGFP fluorescence) and

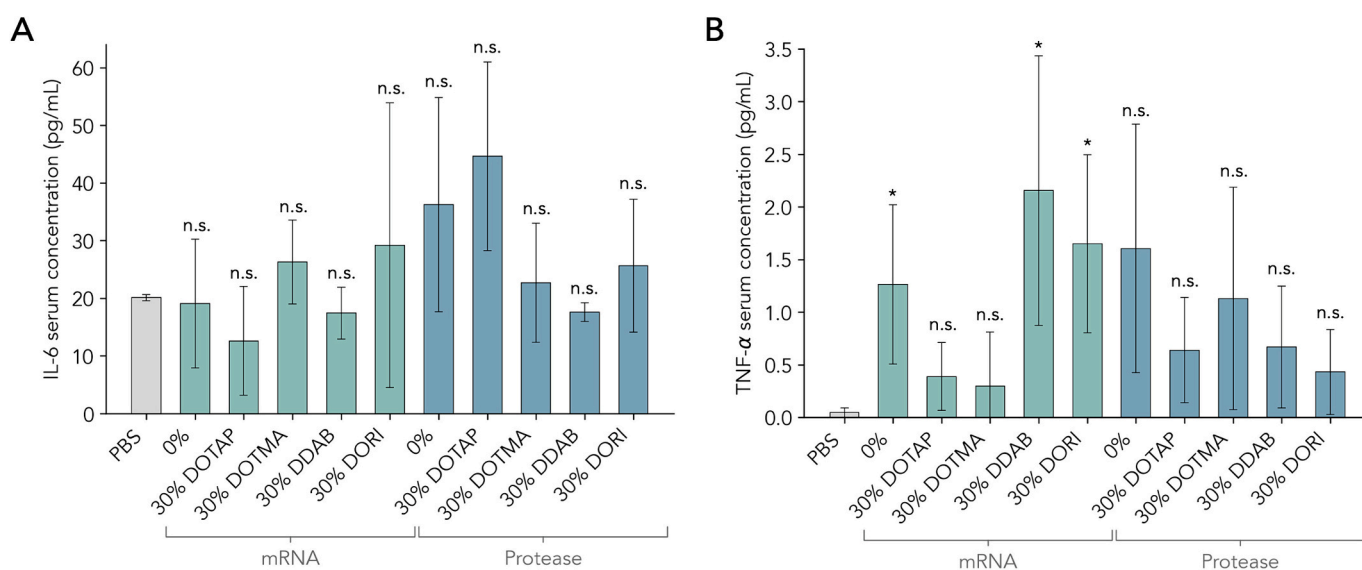


Fig. 6. Cytokine concentrations in mouse serum following treatment with PBS or LNPs encapsulating luciferase mRNA or RAS protease. (A) IL-6 serum concentrations (pg/mL) for PBS and LNPs encapsulating luciferase mRNA or RAS protease. (B) TNF- α serum concentrations (pg/mL) for PBS and LNPs encapsulating luciferase mRNA or RAS protease. $n = 3$. An ANOVA was used to determine if treatment group means differed significantly from the PBS group (*: $p < 0.05$, **: $p < 0.01$, ***: $p < 0.001$).

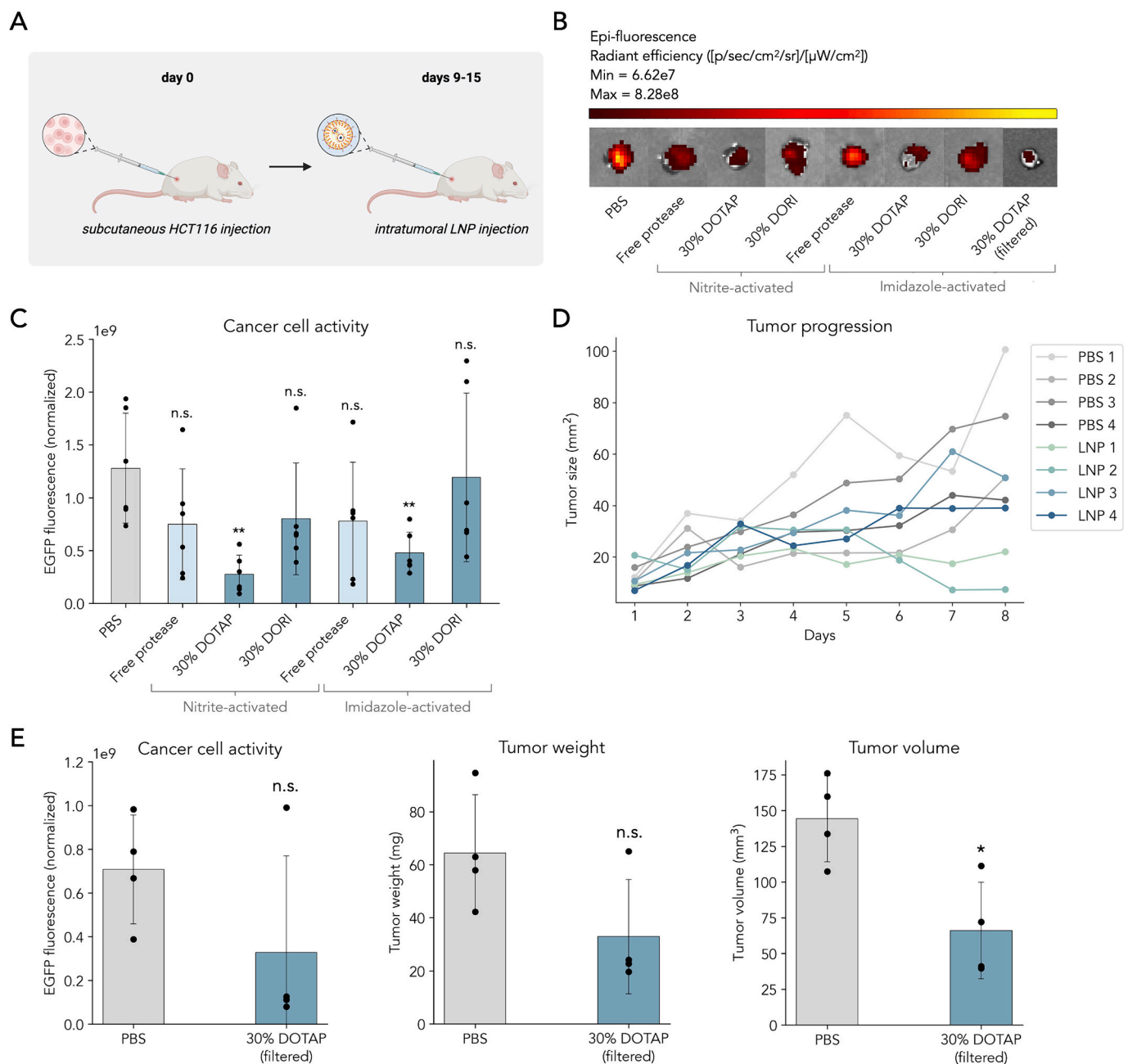


Fig. 7. Normalized EGFP fluorescence and tumor volume following treatment with RAS protease LNPs. (A) Schematic of tumor model experiment. (B) IVIS images of excised tumors. (C) Normalized EGFP fluorescence for groups treated with PBS, or nitrite-activated or imidazole-activated RAS protease (1 mg/kg total protease, free in PBS or within LNP sample). $n \geq 5$ (D) Tumor progression for groups treated with PBS, or imidazole-activated RAS protease encapsulated in the 30% DOTAP formulation and subsequently filtered to remove free protease (0.5 mg/kg total protease). Tumor size was determined by daily caliper measurements and plotted as a single line for each mouse. (E) Normalized EGFP fluorescence, tumor weight, and tumor volume following treatment with PBS or the filtered 30% DOTAP LNP. $n = 4$. Across all graphs, an ANOVA was used to determine if treatment group means differed significantly from the PBS group (*: $p < 0.05$, **: $p < 0.01$, ***: $p < 0.001$).

tumor weight were not statistically significant (Fig. 7E). However, there was still a clear decrease in tumor growth across all metrics tested.

While this delivery platform holds immense potential, the limited encapsulation efficiency indicates that multiple doses over a longer period or co-delivery with existing therapeutics may be required to produce consistent and significant changes in tumor growth and size. However, even with these limitations, this proof-of-concept work shows significant promise, especially if future formulations could be further optimized to improve encapsulation efficiency.

4. Conclusion

In this study, we developed LNPs for intracellular delivery of an engineered protease that specifically cleaves active RAS. Specifically, we tested formulations varying in the concentration and identity of the cationic lipid component to identify potential differences in delivery. LNP formulations with more cationic lipid generally resulted in improved RAS protease encapsulation and delivery efficiency. The top formulations demonstrated a dose-responsive delivery profile *in vitro* and decreased cancer cell proliferation upon activation by imidazole. *In vivo*, both the concentration of cationic lipid and type of cargo influenced LNP and cargo distribution, indicating that published findings

based on cationic lipids may be specific to cargo type. Introducing cationic lipid into all LNP formulations did not significantly affect toxicity at the dosages tested, as measured by serum cytokine levels. Finally, our results suggest that this platform can be used to deliver RAS protease *in vivo* to reduce tumor cell proliferation, as measured by EGFP fluorescence and tumor volume over time.

This work represents a potential advance toward the development of effective, targeted therapeutics for RAS-driven cancers. By successfully delivering RAS protease to cancer cells *in vitro* and *in vivo*, this platform enables the protease to specifically target oncogenic forms of RAS. In future work, further optimization of the delivery vehicle may improve efficacy and allow this approach to be extended to treat other types of cancer. Since the protease cleaves all three isoforms of active RAS *in vitro* [7], LNPs could be optimized to deliver the protease to different tissues and target, for example, KRAS in lung cancer, NRAS in lymphoma, or HRAS in skin cancer. Our *in vivo* biodistribution analysis indicated that RAS protease LNPs with cationic lipid preferentially accumulate in the lungs, suggesting that this platform could be applied to lung cancers.

By inactivating oncogenic RAS, which plays a key role in driving the progression of many cancers, this platform holds potential as a therapeutic for a range of cancers. Combined with future advances in lipid-based delivery systems to further increase efficacy and specificity, this LNP delivery platform could potentially be utilized in therapies for RAS-driven cancers.

CRedit authorship contribution statement

Ella Atsavaprane: Writing – review & editing, Writing – original draft, Investigation, Formal analysis, Data curation, Conceptualization. **Rebecca M. Haley:** Writing – review & editing, Writing – original draft, Investigation, Formal analysis, Data curation, Conceptualization. **Margaret M. Billingsley:** Investigation, Conceptualization. **Alexander Chan:** Investigation, Formal analysis. **Biao Ruan:** Investigation. **Christian G. Figueroa-Espada:** Formal analysis, Data curation. **Ning-qiang Gong:** Investigation. **Alvin J. Mukalel:** Investigation. **Philip N. Bryan:** Writing – review & editing, Resources, Project administration. **Michael J. Mitchell:** Project administration, Funding acquisition.

Declaration of competing interest

None of the authors have conflicting interests to declare.

Data availability

Data will be made available on request.

Acknowledgements

E.A. was supported by a grant from the Blair Undergraduate Research Fund. R.M.H. and A.C. were supported by the National Science Foundation Graduate Research Fellowship Program (NSF-GRFP) under Grant No. DGE-2236662. M.M.B. was supported by a U.S. National Institutes of Health (NIH) Ruth L. Kirschstein National Research Service Award (F31 CA260922). P.N.B. was supported by funding from the NIH (R01 GM141290). M.J.M. was supported by a NIH Director's New Innovator Award (DP2 TR002776), a Burroughs Wellcome Fund Career Award at the Scientific Interface (CASI), an American Cancer Society Research Scholar Grant (RSG-22-122-01-ET), and an NSF CAREER Award (CBET-2145491). Data for this manuscript was generated using the Penn Cytomics and Cell Sorting Shared Resource Laboratory at the University of Pennsylvania and is partially supported by the Abramson Cancer Center NCI Grant (P30 016520, RRid:SCR 022376).

We would also like to acknowledge Dr. Marshall Scott Padilla and Ryann Joseph for assistance with manuscript revisions.

Appendix A. Supplementary data

Supplementary data to this article can be found online at <https://doi.org/10.1016/j.jconrel.2024.05.015>.

References

- [1] D.K. Simanshu, D.V. Nissley, F. McCormick, RAS proteins and their regulators in human disease, *Cell* 170 (2017).
- [2] I.A. Prior, F.E. Hood, J.L. Hartley, The frequency of ras mutations in cancer, *Cancer Res.* 80 (2020).
- [3] A.Q. Khan, et al., RAS-mediated oncogenic signaling pathways in human malignancies, *Semin. Cancer Biol.* 54 (2019).
- [4] A.D. Cox, S.W. Fesik, A.C. Kimmelman, J. Luo, C.J. Der, Drugging the undruggable RAS: Mission possible? *Nat. Rev. Drug Discov.* 13 (2014).
- [5] FDA D.I.S.C.O. *Burst Edition: FDA Approvals of Lumakras (Sotorasib) for Patients with KRAS G12C Mutated Locally Advanced or Metastatic Non-small Cell Lung Cancer, and Truseltiq (Infigratinib) for Unresectable Locally Advanced or Metastatic Cholangiocarcin.* (2021).
- [6] Z.R. Crook, N.W. Nairn, J.M. Olson, Miniproteins as a powerful modality in drug development, *Trends Biochem. Sci.* 45 (2020).
- [7] Y. Chen, et al., Engineering subtilisin proteases that specifically degrade active RAS, *Commun. Biol.* 4 (2021).
- [8] L. Huang, C.M. Counter, Reduced HRASG12V-driven tumorigenesis of cell lines expressing KRASC118S, *PLoS One* 10 (2015).
- [9] B.L. Lampton, et al., Targeting eNOS in pancreatic cancer, *Cancer Res.* 72 (2012).
- [10] K.H. Lim, B.B. Ancrile, D.F. Kashatus, C.M. Counter, Tumour maintenance is mediated by eNOS, *Nature* 452 (2008).
- [11] V.G. Kharitonov, A.R. Sundquist, V.S. Sharma, Kinetics of nitric oxide autoxidation in aqueous solution, *J. Biol. Chem.* 269 (1994).
- [12] K. Pahan, F.G. Sheikh, M. Khan, A.M.S. Nambodiri, I. Singh, Sphingomyelinase and ceramide stimulate the expression of inducible nitric-oxide synthase in rat primary astrocytes, *J. Biol. Chem.* 273 (1998).
- [13] K. Garber, Alnylam launches era of RNAi drugs, *Nat. Biotechnol.* 36 (2018).
- [14] F.P. Polack, et al., Safety and efficacy of the BNT162b2 mRNA Covid-19 vaccine, *N. Engl. J. Med.* 383 (2020).
- [15] L.R. Baden, et al., Efficacy and safety of the mRNA-1273 SARS-CoV-2 vaccine, *N. Engl. J. Med.* 384 (2021).
- [16] J.A. Kulkarni, et al., Design of lipid nanoparticles for *in vitro* and *in vivo* delivery of plasmid DNA. *Nanomedicine nanotechnology, Biol. Med.* 13 (2017).
- [17] T.S. Zatspeyn, Y.V. Kotelevtsev, V. Koteliansky, Lipid nanoparticles for targeted siRNA delivery - going from bench to bedside, *Int. J. Nanomedicine* 11 (2016).
- [18] K.L. Swingle, A.G. Hamilton, M.J. Mitchell, Lipid nanoparticle-mediated delivery of mRNA therapeutics and vaccines, *Trends Mol. Med.* 27 (2021).
- [19] Y. Sasayama, et al., *In vivo* activation of PEGylated long circulating lipid nanoparticle to achieve efficient siRNA delivery and target gene knock down in solid tumors, *J. Control. Release* 311–312 (2019).
- [20] Y. Pei, et al., Sequential targeting TGF- β signaling and KRAS mutation increases therapeutic efficacy in pancreatic Cancer, *Small* 15 (2019).
- [21] B.A. Appleton, et al., Structural studies of neuropilin/antibody complexes provide insights into semaphorin and VEGF binding, *EMBO J.* 26 (2007).
- [22] C.C. Lee, A. Kreuzsch, D. McMullan, K. Ng, G. Spraggon, Crystal structure of the human neuropilin-1 b1 domain, *Structure* 11 (2003).
- [23] Y.C.I. Tsai, et al., Structural studies of neuropilin-2 reveal a zinc ion binding site remote from the vascular endothelial growth factor binding pocket, *FEBS J.* 283 (2016).
- [24] S. Anthiya, et al., Targeted siRNA lipid nanoparticles for the treatment of KRAS-mutant tumors, *J. Control. Release* 357 (2023).
- [25] D. Pramanik, et al., Restitution of tumor suppressor microRNAs using a systemic nanovector inhibits pancreatic cancer growth in mice, *Mol. Cancer Ther.* 10 (2011).
- [26] J.K.W. Lam, M.Y.T. Chow, Y. Zhang, S.W.S. Leung, siRNA versus miRNA as therapeutics for gene silencing, *Molecular Therapy - Nucleic Acids* 4 (2015).
- [27] S. Shen, et al., Cationic lipid-assisted polymeric nanoparticle mediated GATA2 siRNA delivery for synthetic lethal therapy of KRAS mutant non-small-cell lung carcinoma, *Mol. Pharm.* 11 (2014).
- [28] N.J. O'Neil, M.L. Bailey, P. Hieter, Synthetic lethality and cancer, *Nat. Rev. Genet.* 18 (2017).
- [29] A.A. Eltoukhy, et al., Nucleic acid-mediated intracellular protein delivery by lipid-like nanoparticles, *Biomaterials* 35 (2014).
- [30] Y. Rui, et al., Carboxylated branched poly(β -amino ester) nanoparticles enable robust cytosolic protein delivery and CRISPR-Cas9 gene editing, *Sci. Adv.* 5 (2019).
- [31] Q. Cheng, et al., Selective organ targeting (SORT) nanoparticles for tissue-specific mRNA delivery and CRISPR-Cas gene editing, *Nat. Nanotechnol.* (2020), <https://doi.org/10.1038/s41565-020-0669-6>.
- [32] A. Chan, et al., Cytosolic delivery of small protein scaffolds enables efficient inhibition of Ras and Myc, *Mol. Pharm.* 19 (2022).
- [33] R.M. Haley, et al., Lipid nanoparticle delivery of small proteins for potent *in vivo* RAS inhibition, *ACS Appl. Mater. Interfaces* 15 (2023).
- [34] M.M. Billingsley, et al., Ionizable lipid nanoparticle-mediated mRNA delivery for human CAR T cell engineering, *Nano Lett.* (2020), <https://doi.org/10.1021/acs.nanolett.9b04246>.
- [35] M.M. Billingsley, et al., Orthogonal Design of Experiments for optimization of lipid nanoparticles for mRNA engineering of CAR T cells, *Nano Lett.* 22 (2022).

- [36] S.K. Patel, et al., Hydroxycholesterol substitution in ionizable lipid nanoparticles for mRNA delivery to T cells, *J. Control. Release* 347 (2022).
- [37] A.G. Hamilton, et al., Ionizable lipid nanoparticles with integrated immune checkpoint inhibition for mRNA CAR T cell engineering, *Adv. Healthc. Mater.* (2023), <https://doi.org/10.1002/adhm.202301515>.
- [38] S.J. Shepherd, et al., Scalable mRNA and siRNA lipid nanoparticle production using a parallelized microfluidic device, *Nano Lett.* 21 (2021).
- [39] A. Schiefner, A. Angelov, W. Liebl, A. Skerra, Structural basis for cellulose binding by the type a carbohydrate-binding module 64 of Spirochaeta thermophila, *Proteins Struct. Funct. Bioinforma.* 84 (2016).
- [40] M. Kim, et al., Engineered ionizable lipid nanoparticles for targeted delivery of RNA therapeutics into different types of cells in the liver, *Sci. Adv.* 7 (2021).
- [41] K.A. Hajj, K.A. Whitehead, Tools for translation: non-viral materials for therapeutic mRNA delivery, *Nat. Rev. Mater.* 2 (2017).
- [42] K.J. Kauffman, M.J. Webber, D.G. Anderson, Materials for non-viral intracellular delivery of messenger RNA therapeutics, *J. Control. Release* 240 (2016).
- [43] J.S. Suk, Q. Xu, N. Kim, J. Hanes, L.M. Ensign, PEGylation as a strategy for improving nanoparticle-based drug and gene delivery, *Adv. Drug Deliv. Rev.* 99 (2016).
- [44] M. Wang, et al., Efficient delivery of genome-editing proteins using bioreducible lipid nanoparticles, *Proc. Natl. Acad. Sci. USA* 113 (2016).
- [45] S. Omo-Lamai, et al., Physicochemical Targeting of Lipid Nanoparticles to the Lungs Induces Clotting: Mechanisms and Solutions, *bioRxiv*, 2023.
- [46] T. Wei, Q. Cheng, Y.L. Min, E.N. Olson, D.J. Siegwart, Systemic nanoparticle delivery of CRISPR-Cas9 ribonucleoproteins for effective tissue specific genome editing, *Nat. Commun.* 11 (2020).